Published in *Data Analysis and Modeling for Process Control*, ed. Kenneth W. Tobin Jr., Proc. SPIE Vol. 5378 (SPIE, Bellingham, WA) 81-92 (2004).

Comparing the Transient Response of a Resistive-Type Sensor with a Thin-Film Thermocouple during the Post-Exposure Bake Process

Kenneth G. Kreider, David P. DeWitt, Joel B. Fowler, James E. Proctor*,
William A. Kimes, Dean C. Ripple and Benjamin K. Tsai
National Institute of Standards and Technology, Gaithersburg MD 20899
*JEP, Jeptech, Inc., Monrovia, MD

ABSTRACT

Recent studies on dynamic temperature profiling and lithographic performance modeling of the post-exposure bake (PEB) process have demonstrated that the rate of heating and cooling may have an important influence on resist lithographic response. Measuring the transient surface temperature during the heating or cooling process with such accuracy can only be assured if the sensors embedded in or attached to the test wafer do not affect the temperature distribution in the bare wafer. In this paper we report on an experimental and analytical study to compare the transient response of embedded platinum resistance thermometer (PRT) sensors with surface-deposited, thin-film thermocouples (TFTC). The TFTCs on silicon wafers have been developed at NIST to measure wafer temperatures in other semiconductor thermal processes. Experiments are performed on a test bed built from a commercial, fab-qualified track system with hot and chill plates using wafers that have been instrumented with calibrated type-E (NiCr/CuNi) TFTCs and commercial PRTs. Time constants were determined from an energy-balance analysis fitting the temperature-time derivative to the wafer temperature during the heating and cooling processes. The time constants for instrumented wafers ranged from 4.6 s to 5.1 s on heating for both the TFTC and PRT sensors, with an average difference less than 0.1 s between the TFTCs and PRTs and slightly greater differences on cooling.

Keywords: lithographic simulation, platinum resistors, post exposure bake, silicon wafer processing, temperature measurement, thermal modeling, thermometry, thin films, transient response

1. INTRODUCTION

Generally the post-exposure bake (PEB) process consists of exposing process wafers to a set of controlled, steady-state temperature environments. Using commercial test wafers with resistance-type sensors, steady-state temperature measurements are reported to have an uncertainty of 20 mK in the range 15 °C to 230 °C (all uncertainties given as standard uncertainties with coverage factor of k=1) [1]. Such accurate measurements enable the tight temperature control required in order to meet critical dimension (CD) budgets using chemically amplified resists employed in the 130 nm to 70 nm technologies [2].

Recent studies on dynamic temperature profiling and lithographic performance modeling of the PEB process have demonstrated that the rate of heating and cooling may have an important influence on resist lithographic response [1, 2]. Measuring the transient wafer temperature during the heating or cooling process with low uncertainties as can be achieved for steady-state conditions can only be assured if the sensors embedded in or attached to the test wafer do not affect the temperature distribution in the bare wafer. Apart from sensor calibration issues, there are three effects that can result in a reading of an embedded sensor different from the temperature of the surrounding bare wafer surface. First, for a typical heating process, heat transfer analysis predicts that at early times the difference between the lower and upper wafer surface temperatures may be close to 100 mK, whereas the difference at steady-state conditions is close to 5 mK. Second and more importantly, the disturbances caused by the thermal mass of an embedded sensor and by its thermal resistance to the wafer can contribute significantly to the errors in measuring transient surface temperatures. Of course, of practical interest is what effects these measurement errors have on temperature control strategies that eventually influence CD variations.

Published in *Data Analysis and Modeling for Process Control*, ed. Kenneth W. Tobin Jr., Proc. SPIE Vol. 5378 (SPIE, Bellingham, WA) 81-92 (2004).

The temperature-time history or temperature profile of a wafer, initially at room temperature and suddenly subjected to heating when placed in close proximity to the hot plate, can be predicted using the classical heat transfer lumped-capacitance method [3, 4]. The analysis provides the means to calculate the time constant, a measure of the rise time or ramp rate as will be subsequently discussed, in terms of wafer thermal properties, the proximity gap, and other thermal conditions. Smith, *et al.* [1], used the classical model with a lithographic simulation to demonstrate the very large CD variations to be expected with wafers subjected to identical initial and steady-state temperatures, but having time constants different by a factor of two. Cohen, et al. [2], obtained wafer temperature profiles using resistive-type sensors on a production tool for the PEB process and fitted the classical model's exponential temperature-time profile to obtain time constants. Based upon observations on a 14-wafer suite, each with 29 sensors and under identical operating conditions, the average time constant was found as 5.20 s with a standard deviation of 0.11 s.

The purpose of the present study is to characterize the transient performance of resistive-type temperature sensors during the PEB heating process by comparison with measurements using surface-mounted, thin-film thermocouples with negligible thermal mass. Heat transfer models are developed to provide a convenient method for estimating the time constants from the experimentally observed sensor temperature-time profiles as well as to predict the time constant as a function of key system variables, especially the proximity wafer-plate gap and hot-plate temperature. A lithographic simulation is performed using typical experimentally observed temperature-time profiles to demonstrate resulting CD variations with different resists and line densities. A further purpose of the paper is to provide a detailed description of the measurement and analysis methods, including specification of uncertainties. The work is directed toward establishing the traceability and uncertainty of transient measurements in PEB tools using commercial temperature-sensing wafers, which are calibrated in static, isothermal baths.

2. EXPERIMENTAL PROCEDURE

2.1. Test wafer

Our 200 mm test wafers were designed to have four pairs of corresponding thin-film thermocouple junctions and matching commercial platinum resistance thermometers (PRTs) (see Fig. 1). These sensor pairs were placed close to each other (6 mm to 7 mm) in order to measure the 200 mm wafer under nearly identical thermal conditions. We designed and fabricated two wafers with dual instrumentation. One wafer had type-E (Ni/Cr versus Cu/Ni) TFTCs on the wafer surface connected to type-E wires, as well as a set of commercial embedded PRT sensors. Type E thermocouples have high output (50 μV/K to 70 μV/K) and permit lower measurement uncertainty at a high speed of data acquisition. The second dual sensor wafer had thin-film and wire thermocouples of Pt and Pd (5 μV/K to 6 μV/K). Both wafers had embedded thin-film PRTs on 0.25 mm thick alumina substrates secured to the Si wafer with polyimide in a 2.74 mm by 1.43 mm oval shaped hole in the silicon. The PRT sensors were also covered with an AlN-filled polyimide and had 4-wire Pt foil leads.

Fabrication of the dual sensor test wafers started with a 200 mm Si wafer with a 690 nm thick thermal oxide. These wafers were sputter coated with the thin films of Ti bonded Pt and Pd or type-E alloys (Ni-Cr and Cu-Ni). The TFTC wafer fabrication is described in more detail in references [5, 6]. For the PEB test wafers the connections between the matching thin films and thermocouple lead wires were made with silver epoxy on the bond pads of the wafer except for the Pt connections, which were made with PbSn solder.

This design permits the metallurgically bonded thin-film thermocouple junction to be essentially massless because it is 1 μm thick compared to the 0.76 mm thick wafer. We have measured the response times of the thin film junctions [7] and found them to be <5 ms. The thin-film thermocouple is used as a differential thermocouple between the measuring junction and the interface with the wire thermocouple. We calibrated the thin-film thermocouples using the comparison method described in Ref. [8]. Since this temperature difference is less than 5 °C the measurement is not very sensitive to the calibration accuracy of the thin-film thermocouple. The wafers instrumented with both PRTs and TFTCs are designed to compare the transient response of the two types of sensors and not their absolute temperature measurement. In fact, the PRTs have smaller temperature measurement uncertainties than the thin-film thermocouples.

Published in *Data Analysis and Modeling for Process Control*, ed. Kenneth W. Tobin Jr., Proc. SPIE Vol. 5378 (SPIE, Bellingham, WA) 81-92 (2004).

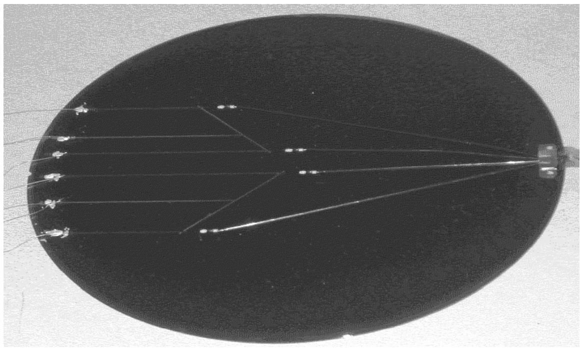

Figure 1. Wafer instrumented with PRTs and type-E thin film thermocouples.

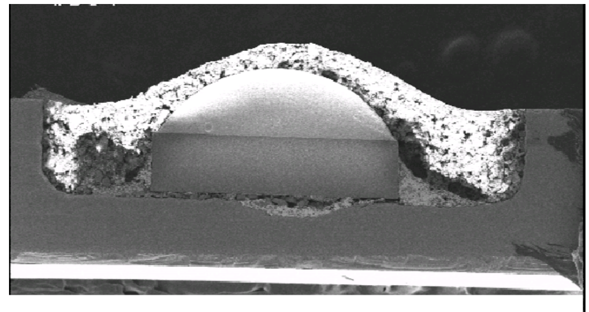

[⇐ 600 μm ⇒]

Figure 2. Cross section of a PRT as seen using an electron microscope.

We cut cross sections of two of the PRTs on the 200 mm instrumented wafer. Figure 2 is an electron microscope image of the cavity in the Si wafer (above the white line) containing an Al_2O_3 substrate which holds the thin-film PRT and a "dome" of high thermal conductivity polyimide cover. The assembly is cemented into the drilled pit in the Si wafer and covered with a filled polyimide (white color). The gap between the Al_2O_3 substrate and the Si wafer is approximately 25 μm wide and can be measured using the scale on the figure. The Si pit also has a dip where the gap is larger. The electron microscope image of the second sensor displayed a slightly larger gap.

2.2. PEB track

The PEB test bed (Fig.3) consisted of a stationary hot plate with moving placement pins and a hot plate cover, and a movable water-cooled chill plate. The hot plate cover moved vertically. The hot plate cover had a distance of 40 mm from the bottom of the cover to the hot plate when raised and 5 mm when closed. The positioning pins would rise 18.5 mm above the hot plate to allow the chill plate to slide under the wafer. The chill plate had two slots, which would allow the three positioning pins to move freely through the chill plate. The hot plate was heated using 208 VAC with a zero-cross-firing SCR, which was controlled using a PID controller. The PID control system controlled the hot plate with a stability of ±1°C. Our measurements indicated that the hot plate had a temperature uniformity of better than 1.5 °C across the entire surface. The chill plate was chilled by circulating water from a refrigerated water bath held at 20 °C. The hot plate and chill plate each had six, 100 µm ±10µm high ceramic spacers, consisting of a 100 µm high base and a tapered ceramic retainer (Fig. 4). The base of the spacers controlled the size of the air gap between the wafer and the hot or chill plate, thereby controlling heating or cooling of the wafer via thermal conduction through the gap. The tapered retainers of the spacers controlled the lateral position of the wafer to within 0.7 mm on the hot and chill plates.

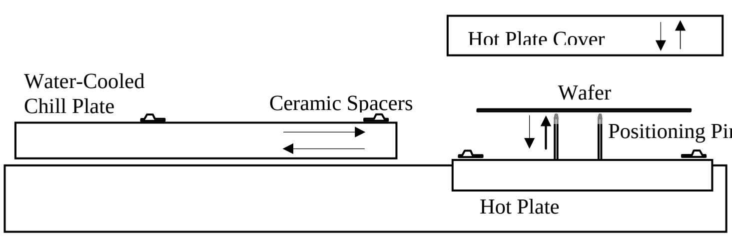

Figure 3. A diagram of the PEB test bed.

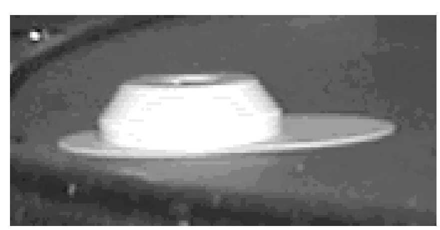

Figure 4. A 100 µm ceramic spacer with tapered pedestal.

Published in *Data Analysis and Modeling for Process Control*, ed. Kenneth W. Tobin Jr., Proc. SPIE Vol. 5378 (SPIE, Bellingham, WA) 81-92 (2004).

The cover, chill plate and positioning pins were moved using pneumatic actuators. The test bed was controlled using a custom computer program. The procedure for heating and cooling the wafer was as follows: The wafer began on the chill plate, with the chill plate positioned above the hot plate. The positioning pins would rise up from the hot plate, lifting the wafer off of the chill plate. The chill plate would then retract away from the wafer and hot plate. The placement pins would move back into the hot plate, placing the wafer onto the ceramic spacers on the hot plate. The hot plate cover would descend covering both wafer and hotplate. Once the heating cycle was complete the cover would lift off of the hot plate, uncovering the wafer. The positioning pins would then rise up out of the hot plate, lifting the wafer. Finally, the chill plate would slide underneath the wafer, and the positioning pins would descend, placing the wafer onto the chill plate. Throughout this process the wires were draped as to minimize their force exerted on the wafer.

2.3. Instrumentation

Six 8 1/2 digit multimeters were used to read the sensors on the specially instrumented test wafers. In order to sample the multiple sensors of the test wafers at an adequate rate, a single multimeter was used for each sensor. Each multimeter had an uncertainty of less then 0.5 μV for DC voltage measurements and 3 mΩ for the resistance measurements. The PRTs were read using a four-wire resistance measurement with a common current sink for all the sensors. The voltage from each wire thermocouple was read independently from the thin-film thermocouples. The cold junctions for the thermocouples were placed in glass tubes extending into a Dewar filled with a shaved ice and water slurry. Copper leads connected the cold junctions to the multimeter input terminals. Each multimeter took one reading every 0.1 s, synchronized and triggered by an external TTL signal generated 1.5 s before the pins placed the wafer onto the hot plate. For each thermal cycle, measurements were taken over a period of 100 s. The data were stored in the multimeter memory and extracted following the thermal cycle using a custom computer program.

A custom computer program was also written to record the temperature of the hotplate throughout each thermal cycle of the wafer, as well as to monitor and note any triggering of the PEB bed's pneumatic actuators.

3. EXPERIMENTAL RESULTS

Forty-two PEB test bed cycles with the 200 mm wafers using both thermocouple and Pt resistance thermometer (PRT) sensors were measured. Each test was accomplished with two of the four type-E thin-film thermocouple (TFTC) junctions and the adjacent two of the four PRTs. The thermocouple measurements required four multimeters to read both the wire thermocouples combined with the TFTCs and the TFTCs alone.

The tests were planned to investigate the effect of various temperatures (100 °C to 150 °C), various rotational positions of the test wafer, various sensor locations (near center and at mid-radius), various wafer to hotplate gaps (0.10 mm and 0.13 mm), and two different thermocouples (type-E and Pt/Pd). The tests also included some redundancies on different days.

A typical thermal cycle is depicted in Fig. 5, where the differential TFTC output is indicated by the open diamonds, the lower thin black line indicates the output of the thin film and the wire thermocouples, and the PRT temperature is indicated by the thin upper black line. The activities of the PEB track pneumatic actuators are indicated by the dashed line pillars and the upper most solid line indicates the temperature of the hotplate. The thin film output is indicated by the y-axis to the right. The left y-axis indicates the temperature of the PRT, the hotplate, and the sum of the wire and thin film thermocouples.

Published in *Data Analysis and Modeling for Process Control*, ed. Kenneth W. Tobin Jr., Proc. SPIE Vol. 5378 (SPIE, Bellingham, WA) 81-92 (2004).

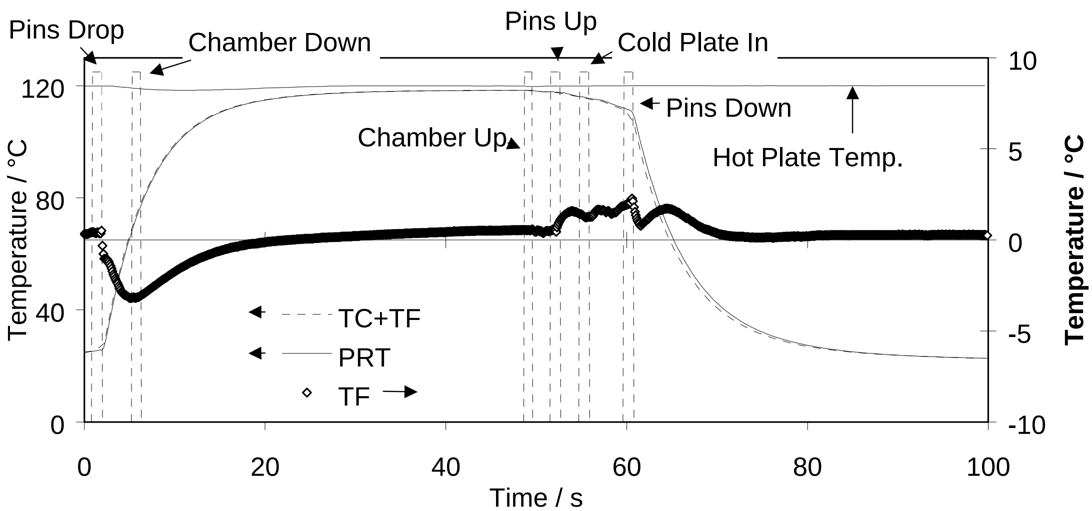

Figure 5. Wafer instrumented with type-E thin film thermocouples and PRT. Heated using the PEB bed hotplate set at 120 °C.

A thermal cycle begins when the placement pins lift the wafer from the chill plate. The data collection process starts immediately before the placement pins began to descend, which place the wafer onto the hotplate spacers. Once the placement pins are fully lowered the temperature of the wafer quickly begins to rise, as indicated by the sharp change in slope of the solid lines in Fig. 5. As the wafer was heated the output of the TFTCs decreased, indicating the edge of the wafer was hotter then the mid-radius. The measured temperature of the TFTC junction and the PRTs began to diverge slightly, with the TFTC junctions reading slightly warmer then the PRTs. The presence of the cold wafer decreased the temperature of the hot plate, as seen by the top solid line in Fig. 5. After the wafer was placed on the hotplate spacers the cover of the chamber descended, covering the wafer and hot plate. At almost the same time as the chamber door descends an inflection point in the thin film output develops, indicating the mid-radius of the wafer was heating up relative to the periphery. This inflection point did not always occur as the chamber door descended. The thin films, PRTs and hot plate proceeded to heat up, with the PRT temperature trailing the temperature of the thin film junctions slightly. As the wafer approached the steady state condition the measured temperature of the thin film junction and the PRT converged to a temperature slightly less then the set point of the hotplate.

Once both the PRTs and the TFTCs had reached thermal equilibrium we lifted the chamber door, which slowly began to cool the wafer. This initial cooling was very symmetric across the wafer, which meant there was very little change in the output of the thin films. The placement pins lifted the wafer off the hot plate, increasing the cooling rate of the wafer. At this point there was a slight increase in the output of the thin films, indicating that the temperature at the mid-radius of the wafer was warmer than the periphery. At this stage in the cooling process the temperature of the thin films and the PRTs began to diverge slightly, with the thin films reading slightly cooler then the PRTs. The placement pins then descended, placing the wafer onto the cool plate. Once placed on the cool plate the temperature of the wafer changed rapidly, resulting in a sharp change of slope in the measured temperature and an increase in the thin film outputs. While cooling, the temperatures of the thin films and PRTs diverged, with the time constant of the PRTs exceeding that of the thin films by about 0.3 s. As the wafer approached steady state conditions the measured temperature of the thin films and the PRTs converged.

The difference in response time of the wafer heating and cooling processes is indicated in Fig. 6 for a typical run. In both heating and cooling the thin films reacted more quickly to their surrounding thermal environment than the PRTs. The difference between the response times of the sensors was greater in cooling than in heating.

Published in *Data Analysis and Modeling for Process Control*, ed. Kenneth W. Tobin Jr., Proc. SPIE Vol. 5378 (SPIE, Bellingham, WA) 81-92 (2004).

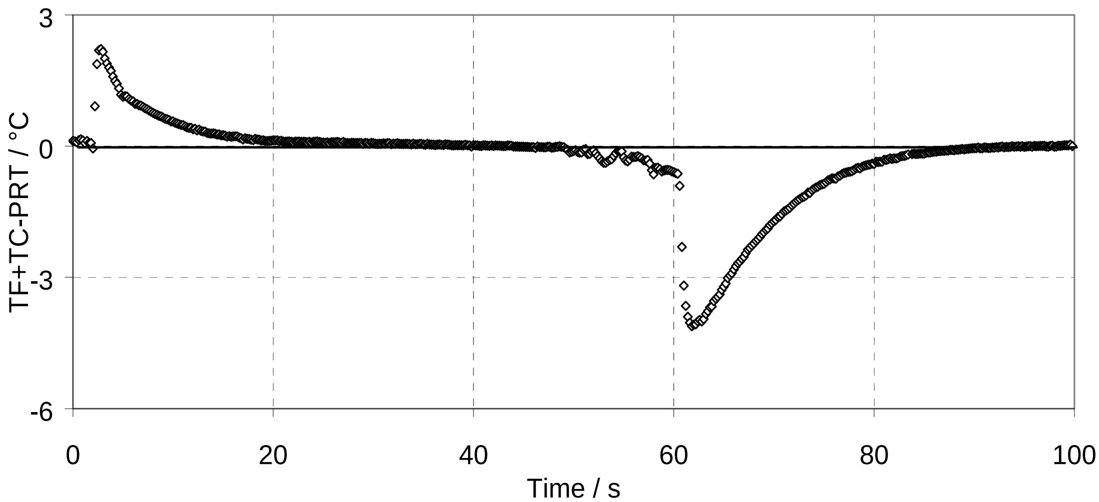

Figure 6. The difference between the temperature of the sum of the thin film plus wire thermocouple and the PRT during the thermal cycle shown in Fig. 5.

Forty-two thermal cycles were performed on two different wafers at three different hot plate temperatures, 100°C, 120°C and 150°C. Of the 42 thermal cycles, 24 were done using the wafer instrumented with a type-E thin films and thermocouples and 18 were performed with the wafer instrumented with the Pt/Pd thin films and thermocouples. Eleven thermal cycles, out of the 42, resulted in the thin films measuring a thermal gradient of greater than 10°C from the periphery of the wafer to the mid-radius, indicating the wafer was poorly seated on the ceramic spacers. The data from these 11 poorly seated thermal cycles were not used in the analysis.

The response time of the Pt/Pd wafer was similar to the type-E wafer. The only appreciable difference was the scatter in the Pt/Pd data because of the inferior signal (5 μV/°C versus 50 μV/°C) to noise ratio.

Two thermal cycles were performed where with the type-E wafer rotated 5° counter clockwise and two thermal cycles were performed where the wafer was rotated 180°. These were done to determine the effect of wafer warpage, repositioning of the sensors relative to the hot plate, and repositioning of the wire leads. The only appreciable difference between the measurements done at 0° rotation, and 5° or 180° was a slightly higher standard deviation on each run.

Three thermal cycles were performed with the type-E wafer while monitoring one center thin film versus the adjacent PRT and one mid-radius thin film versus its PRT. The heating portion of the center sensors showed little significant difference between the mid-radius sensors. On these thermal cycles only the heating portion of the center PRT and thin film were usable because of the close proximity of the center sensors to the slots in the cool plate.

Of the 18 thermal cycles performed using the Pt/Pd wafer, nine were done using the 100 µm spacers. The remaining nine thermal cycles were done after inserting a 0.03 mm aluminum shim between the ceramic spacer and the hot plate. This resulted in a much slower response time of the sensors.

4. MODELING AND ANALYSIS

Heat transfer models were developed to estimate the time constant of the wafer during the heating process based upon the properties of the wafer, thermal conditions and characteristics of the hot plate and determined from the observed experimental temperature-time history.

Published in *Data Analysis and Modeling for Process Control*, ed. Kenneth W. Tobin Jr., Proc. SPIE Vol. 5378 (SPIE, Bellingham, WA) 81-92 (2004).

The hot plate, cover and wafer are represented in Fig. 7. The wafer, initially at a uniform temperature, T_i, is suddenly placed in close proximity to the hot plate at a temperature T_{hp} while exposed to the cover at a temperature T_{cv}. Because the lower and upper air gaps are small, and the temperature differences are moderate, the Rayleigh number is quite small and heat transfer at both surfaces occurs by conduction rather than by convection. Assuming the wafer is isothermal, the energy balance considering the conduction processes and the rate of change of internal energy [1] has the form

$$-\frac{k_{air}}{\delta}\left(T-T_{hp}\right)-\frac{k_{air}}{d}\left(T-T_{cv}\right)=\rho cL\frac{dT}{dt} \tag{1}$$

where the relevant thermophysical properties are the thermal conductivity of air, k_{air}, and the density, ρ, and specific heat, c, of the wafer (silicon). From knowledge of the thermal conditions (T_i, T_{hp}, and T_{cv}) and the physical dimensions of the system (δ =0.1 mm, L = 0.783 mm, d = 5 mm), the energy balance can be numerically integrated to obtain the temperature-time history, $T(t)$. The thermophysical properties, k_{air} and c, generally depend on the air and wafer temperature, respectively. The time constant, τ, can be determined from knowledge of $T(t)$ as the time at which the temperature ratio, $\vartheta(t)$, has the value of 1/e

$$\vartheta\left(t\right)=\frac{T\left(t\right)-T_{ss}}{T_i-T_{ss}}=1/e \tag{2}$$

where T_{ss} is the steady-state temperature. Referred to as the *dual resistance-capacitance (RR-C) model*, we have considered the thermal resistances of the two conduction processes and the thermal capacitance of the wafer. The internal thermal resistance of the wafer is negligible relative to the external thermal resistances thereby justifying the wafer isothermal assumption; that is, the Biot number is much less than unity [4].

Because conduction from the hot plate to the wafer dominates the heating process, the forgoing analysis can be simplified by neglecting the heat transfer to cover. The energy balance of Eq. (1) can be written as

$$-\frac{\left(T-T_{hp}\right)}{R_t''}=C_t''\frac{dT}{dt} \tag{3}$$

in terms of the thermal resistance per unit area of the hotplate conduction process and the thermal capacitance per unit area of the wafer, respectively,

$$R_t''=\frac{\delta}{k_{air}} \qquad \text{and} \qquad C_t''=\rho cL \tag{4, 5}$$

the thermophysical properties as constants evaluated at the average temperature of the heating process, and assuming that T_{hp} is a constant temperature, the differential equation can be analytically integrated to obtain the temperature-time history

$$\frac{T\left(t\right)-T_{hp}}{T_i-T_{hp}}=\exp\left(-\frac{t}{\tau}\right) \tag{6}$$

where the time constant is product of the thermal resistance and capacitance,

$$\tau=R_t''C_t'' \tag{7}$$

Referred to as the *simple resistance-capacitance (R-C) model*, we learn that the temperature-time history will have an exponential form as has been demonstrated by earlier investigations.

The data indicated that T_{hp} cannot be reasonably treated as a constant as the wafer temperature approaches the hot plate temperature, and the integration of Eq. (3) must be done numerically. Alternatively, the energy balance of Eq. (3) provides a convenient method for estimating the time constant from the experimentally observed temperature-time history during the heating process. Assume that the thermal resistance and capacitance parameters are constants and rearrange the terms,

$$\left(\frac{dT}{dt}\left(t\right)\right)=-\frac{1}{R_t''C_t''}\left(T\left(t\right)-T_{hp}\right) \tag{8}$$

Note that the temperature-time derivative, (dT/dt), is a linear function of the wafer temperature difference, ($T-T_{hp}$), and, from Eq. (7), the slope is the reciprocal of the time constant. The slope and linear regression statistics, including the

Published in *Data Analysis and Modeling for Process Control*, ed. Kenneth W. Tobin Jr., Proc. SPIE Vol. 5378 (SPIE, Bellingham, WA) 81-92 (2004).

statistical uncertainty of the slope, were obtained by fitting Eq. (8) to data for each run by the method of least squares. Figure 8 illustrates this linear behavior; the time constant is determined from the slope.

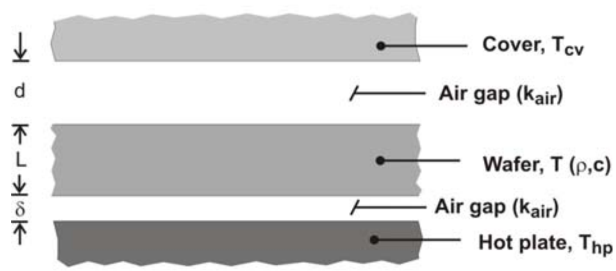

Figure 7. Modeling the wafer during the heating process.

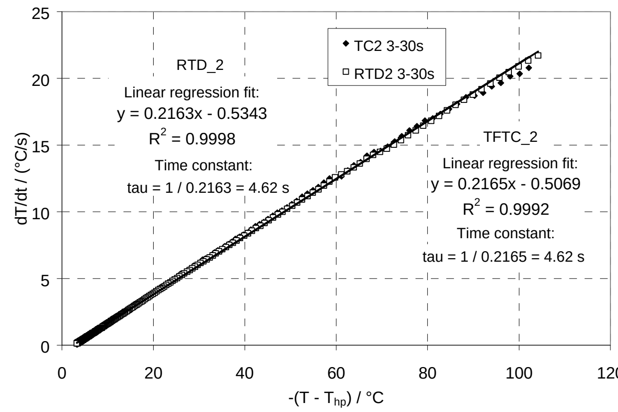

Figure 8. The temperature-time derivative appears as linear function of the wafer temperature difference so that the slope is the reciprocal of the wafer time constant.

5. DISCUSSION OF RESULTS

The time constants (τ) for the heating process on wafer #1 (Type-E TFTCs) for hot plate temperatures of 100 °C, 120 °C and 150 °C with the standard proximity gap of 100 μm are summarized in Table 1. The TFTC and PRT sensors labeled 1 and 2 are located at the mid-radius locations as shown earlier in Fig. 1, except one case identified below.

The sets A, B and C represent a complete family of experiments at the three hot plate temperatures. The time constants and the standard deviations at each hot plate temperature are based upon the average of three runs, except for set B which represents two repeated runs. Comparisons of the time constants determined from TFTC and PRT observations show two major features. First, for all the conditions (except for TFTC2 and PRT2, set B), the time constant from the TFTC observations are lower than those from the PRT sensors. The difference ranges from 0.02 s to 0.04 s, which is about the magnitude of the standard deviations for the differences. Second, the time constants for both sensors decrease with increasing hot plate temperature, about 3 % between the 100 °C and 150 °C operating temperatures.

The data set D represents the average of five runs at a hot plate temperature of 150 °C in which the orientation of the wafer was rotated 5° (1 run) and 180° (2 runs) relative to the standard position (0°, 2 runs) used in sets A – C. For this set, the average time constants are nearly identical to those with the standard position, set C, and the differences between the time constants determined from the two sensors are about the same magnitude. Note however that for TC1 and PRT1, the standard deviations for the time constants are nearly 3 to 4 times larger than for the standard set, which may be an indication that the sensor wire leads likely caused some disturbances or a consequence of alterations in the proximity-gap thermal resistance from relative rotations of the array of holes in the hot plate.

The data set E represents the average of three runs at a hot plate temperature of 150 °C in which the TC1 and PRT1 sensors are located at the center of the wafer (see Fig. 1) while the TC2 and PRT2 sensors located at the wafer mid-radius, as was the condition for all the foregoing data sets. Note that the time constants and their standard deviations for the TC2 / PRT2 sensors replicate well the results for C and D data sets. However, for the time constants for the TC1 / PRT1 sensors are higher than for the C and D sets, probably a consequence of the array of holes in the hot plate that alter the proximity gap thermal resistance.

Published in *Data Analysis and Modeling for Process Control*, ed. Kenneth W. Tobin Jr., Proc. SPIE Vol. 5378 (SPIE, Bellingham, WA) 81-92 (2004).

Table 1. Time constants determined from TFTC (Type-E) and PRT sensor observations on Dual Wafer #1 with standard gap separation. (τ)

		Time constant, s / Standard deviation, s					
Set	T_{hp} (^oC)	TC1	PRT1	PRT1-TC1	TC2	PRT 2	PRT2-TC2
A	100	5.06	5.02	-0.04	5.10	5.08	-0.03
		0.06	0.02	0.04	0.04	0.01	0.03
B	120	4.93	4.89	-0.03	4.94	4.92	-0.02
		0.04	0.04	0.00	0.03	0.02	0.01
C	150	4.66	4.66	0.00	4.58	4.62	0.03
		0.05	0.03	0.03	0.05	0.01	0.04
D	150	4.60	4.64	0.04	4.46	4.56	0.10
		0.15	0.17	0.02	0.04	0.06	0.03
E	150	4.76*	4.82*	0.06	4.43	4.58	0.12
		0.02	0.00	0.02	0.02	0.02	0.01

* Sensors are located at wafer center, rather than at the mid-radius location.

Table 2. Time constants (τ) determined from TFTC (Pt-Pd type) and PRT sensor observations on Dual Wafer #2 with standard and extended proximity gaps.

		Time constant, s / Standard deviation, s					
Runs	T_{hp} (^oC)	TC1	PRT 1	PRT1-TC1	TC2	PRT2	PRT2-TC2
Standard proximity gap (100 µm)							
F	100	5.03	5.17	0.13	4.98	5.06	0.08
		0.06	0.01	0.07	0.06	0.03	0.04
G	120	4.83	4.98	0.14	4.79	4.84	0.06
		0.03	0.01	0.03	0.03	0.00	0.03
H	150	4.68	4.81	0.12	4.64	4.69	0.04
		0.10	0.14	0.04	0.09	0.13	0.04
Extended proximity gap (133 µm)							
I	100	7.38	7.32	-0.06	*	7.51	---
		0.15	0.06	0.09		0.07	---
J	120	7.06	7.05	-0.01	*	7.23	---
		0.05	0.02	0.03		0.02	---
K	150	6.75	6.74	-0.01	*	6.91	---
		0.01	0.01	0.01		0.02	---

* Sensor failed during this series of experiments.

The time constants for the heating process on wafer #2 (Pt-Pd type TFTCs) for hot plate temperatures of 100 °C, 120 °C and 150 °C with the standard proximity gap of 100 µm and the extended gap of 133 µm are summarized in Table 2. Considering the standard proximity gap data sets F, G and H, each representing the average of three runs, the time constants determined from the different sensors show the same general features as those on wafer #1. However, because the Seebeck coefficient of the TFTCs is nearly an order of magnitude lower than for those on type E wafer, the signal noise is greater and as expected the standard deviations of the TFTC time constants are significantly larger, by about a factor of two. For the extended proximity gap data sets I, J, and K, the time constants increase markedly as the thermal resistance of the proximity gap has been increased by about 30 %. The differences between the TC1 and PRT1 time constants can be barely discerned given the standard deviations of the averages. Note that the time constants for PRT2 are higher, about 0.2 s, than those for PRT1, probably as a consequence of non-uniform proximity gap resulting from dimensional variability of the 0.03 mm shims under the proximity pads.

The time constants from the data sets A-C and I-K for the standard and extended proximity gap distances, respectively, and hot plate temperatures of 100 °C, 120 °C and 150 °C are compared with estimates from the heat transfer models described earlier. In Fig. 9, the lower data points are for the standard gap, 100 µm using the R-RC model. The R-C model predicts a lower time constant than determined from the observations, and does not represent the temperature dependence as well as does the R-RC model. The best fit between the model and the experimental results is obtained with a proximity value of 110 µm. The manufacturer's specification for the standard gap uncertainty is 10 %, making the fitted gap distance a reasonable outcome. In Fig. 9, the upper data points are for the extended gap, which was obtained by inserting aluminum foil shims (about 33 µm) under the ceramic pads. The R-RC model fits the data best with a proximity gap of 160 µm, rather than a value expected to be closer to 143 µm. However, the R-RC model represents the temperature dependence of the time constants for both the standard and extended proximity gaps showing consistency between the experimental and modeling approaches.

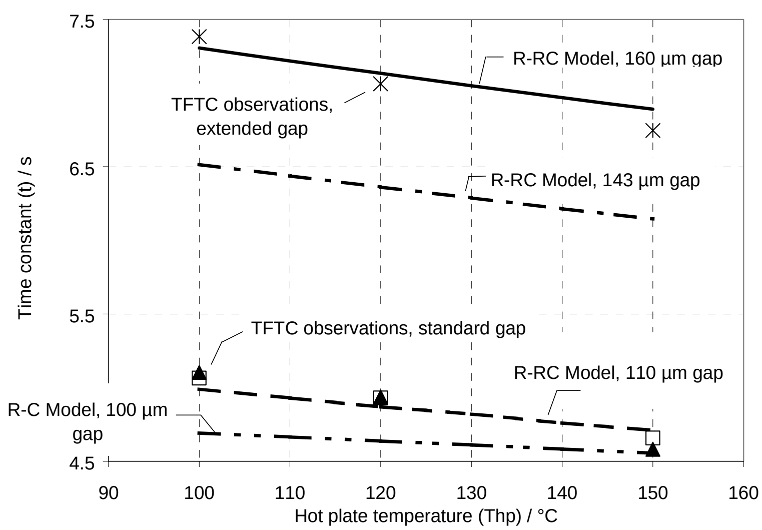

Figure 9. Comparison of experimentally determined time constants with those determined by the R-C and R-RC models.

The statistical uncertainties in the time constants determined from the energy balance method are determined from the statistics provided with the linear regression analysis. An important condition imposed on the analysis is the time span over which the linear fit is regressed. For all the standard proximity gap data sets, the time interval is 3 s to 30 s; for the extended proximity gap sets (I-K), with the longer rise time, the time interval is chosen as 3 s to 40 s. Altering this time interval can introduce changes in the apparent time constant as high as 30 %, although this change is correlated for both the PRT and TC data and the results for relative responses of the PRTs and TCs are not appreciably altered. For the data sets A-E (wafer #1, Type-E), the standard statistical (Type A) uncertainty for the time constant is less than 0.01 s for each individual run, a consequence of the linear fits having very high *r*-squared values, typically greater than 0.999. For the data sets F-H with wafer #2 (Pt-Pd type), the standard error is 0.02 s to 0.03 s for the TFTCs, but remains at 0.01 s for the PRT sensors. For the data sets I-K, with the extended gap, the signal noise from the TFTCs increases even more and the standard error is now 0.03 s to 0.05 s, while again the standard error associated with the PRTs remains at 0.01 s.

The transient response shown in Fig. 6 is a result of the PRTs lagging the TFTCs by approximately 0.2 s in the early stages of the heating and cooling processes. This lag time is actually consistent with the much smaller differences observed between the PRT and TFTC time constants for the wafer temperature. Numerical simulations of heating curves expected from a sensor response time of 0.2 s compared with that from a sensor response time of 0 s gave differences of <0.01 s for the wafer time constant on heating.

Simulation of the lithography process provides a tool to understand the effect of temperature profile on PEB metrology sensitivities. Petersen [9] selected four existing resist parameter sets with a range of line-width critical dimension (CD) sensitivity and typical imaging conditions for a 90 nm imaging technology. The objective of the simulation was to show the variation of the line-width on a wafer resulting from a typical experimental data set for the thin-film thermocouple and resistance sensors, designated subsequently as sensors A and B, respectively. Their temperature profiles are similar to that shown in Figure 5 and their heating time constants are 4.96 and 4.92 s, respectively. Table 3 identifies the PEB sensitivities for the four resists and the exposure dose for the CD variation outcomes corresponding to a 90 nm linewidth sensitivity condition and 1:1 line features (dense).

Table 3 Lithography simulation predicting line-width variations resulting from different sensor temperature profiles.

Resist	PEB sensitivity (nm/°C)	Sensor A Reference line width (nm)	Linewidth difference (%)	
			Sensor B	Sensor B with bias*
1	2.1	89.9	0.2	1.4
2	4.3	89.8	1.1	8.7
3	9.0	89.8	1.6	12.4
4	23.3	90	12.2	50.6

*Linear basis is zero at initial wafer temperature and ±0.25 °C at maximum temperature.

The column labeled Sensor A line-width identified the resulting line-width for the four different resists using the thin-film thermocouple temperature profile. The last two columns are the line-width differences (nm) resulting from the temperature profile of the PRT sensor B and from the profile corrected with a linear bias of ±0.25 °C (that is, no bias at room temperature, and a linear bias changing with wafer temperature to a maximum of ±0.25 at the steady-state temperature).

Total line-width budgets of ±10% are often used as a constraint for forming circuitry into the finished semiconductor product. These budgets are arbitrary and are actually determined by the need of the device being fabricated. This budget is consumed by variations in the mask, exposure tool, resist, substrate, resist processing, etch and subsequent processing. This means that the budget for a thermally activated chemically amplified resist that can be consumed by the post-exposure bake is around 0.5% to 2% of the 10%. If the bake's constraint is set to budget ≤1% then sensor B accuracy would be acceptable for Resist 1 but not for the others. However if the precision of B were ±0.25 °C then these results show that sensor B would fail even with Resist 1. Further, the results shown here are for one type of feature and imaging process, as such it is critical to note that these results represent only a subset of the cases actually encountered in the fab. To gain more clarification it is important to look at more feature types using more critical resist and process parameters.

6. CONCLUSIONS

We measured the temperature of 200 mm Si wafers in a commercial type PEB track using both embedded PRTs and thin-film thermocouples (TFTCs). This instrumented wafer was thermally cycled from a chill plate to the PEB hot plate and back to the chill plate. The sensors were read at 0.1 s intervals for 100 s. We were able to follow the surface temperature of the wafer with the TFTCs with better than 0.1 s resolution.

Our measurements of the time constants for heating 200 mm instrumented wafers in the PEB track gave values of 4.6 s to 5.1 s using both commercial PRTs and TFTCs. The transient response of the TFTCs led the PRT sensors indicating a PRT lag of up to 2 °C on heating and up to 4 °C on cooling for several seconds. The wafer time constants for response were strongly affected by the air gap distance between the wafer and hot plate as expected. The response times of the wafers were slower at lower hot plate temperatures (100 °C) as would be expected because of the lower thermal conductivity of air. Thermal models were presented that showed estimates for heating time constants in good agreement with experimental data using the gap distance as an adjustable parameter. Lithography simulation results were presented showing effects of experimental and analytical bias temperature profiles on CD variations.

ACKNOWLEDGMENTS

The authors wish to acknowledge the contributions of Sensarray Inc. in supplying the PEB track and PRT instrumented wafers [10]. We also appreciate the electron microscope investigation by C. B. Montgomery, NIST.

REFERENCES

1. M.D. Smith, C.A Mack and J.S. Petersen, “Modeling the impact of thermal history during post-exposure bake on the lithographic performance of chemically amplified resists,” Proc. SPIE 4345, pp 1013-1021 (2001).

2. B. Cohen, M. Sun, W. Renken and P. Miller, “Accurate measurements of temperatures in the DUV post exposure bake process,” Proceedings of 8th Symposium on *Temperature: Its Measurement and Control in Science and Industry*, D.C. Ripple ed., AIP Conference Proceedings, pp. 1075-80, (2003).

3. N. Ramanan, F.F. Liang and J.B. Sims, “Conjugate heat-transfer analysis of 300mm bake station,” Proc. SPIE 3678, pp 1296-1306 (1999).

4. F.P. Incropera and D.P. DeWitt, *Fundamentals of Heat and Mass Transfer*, Wiley, 5th ed., 2002. Sects. 5.1-5.3.

5. K.G. Kreider “Temperature calibration Wafer for Rapid Thermal Processing using Thin-film Thermocouples” U.S. Patent 6,037,645, Mar. 14, 2000

6. K.G. Kreider and G.J. Gillen, “High Temperature materials for thin-film thermocouples on silicon wafers,” Thin Solid Films, **376**, 32-37 (2000).

7. D.R. Burgess, Jr., K.G. Kreider, and M. Yust, “Transient thermal response of plasma-sprayed zirconia measured with thin film thermocouples,” Sensors and Actuators, **A 24**, 155-161 (1990).

8. K. G. Kreider, D. C. Ripple and D.P. DeWitt, “Calibration of thin-film thermocouples on silicon wafers,” in *Proceedings of TEMPMEKO99: the 7th International Symposium on Temperature and Thermal Measurements in Industry and Science*, June 1999, Delft, NL. pp. 286-291.

9. J. S. Petersen, Petersen Advanced Lithography, Inc., Austin, TX, Personal Communication with DPD, Jan 10, 2004; analysis used PAL’s ProLE^{TM} simulator incorporating KLA-Tencor’s PROLITH^{TM} lithography simulator.

10. The mention of commercial products by name does not in any way indicate their endorsement by NIST.